Supplementary Information

Co-gel strategy for preparing hierarchically porous silica/polyimide nanocomposite aerogel with thermal insulation and flame retardancy

Xinhai Zhang, [a] Xingxing Ni, [a] Chenxi Li, [a] Bo You, *[a] and Gang Sun [b]

[a] Department of Materials Science, Advanced Coatings Research Center of Ministry of Education of China, Fudan University, Shanghai 200433, People's Republic of China.

[b] Department of Aeronautics and Astronautics, Fudan University, Shanghai 200433, People's Republic of China.

 Corresponding author: Bo You

 Corresponding Author E-mail: youbo@fudan.edu.cn

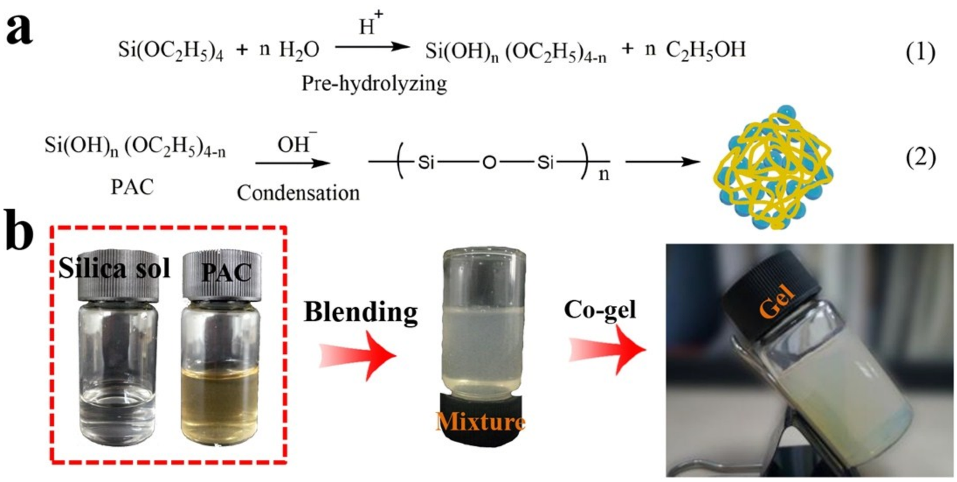

Figure S1. (a) Hydrolysis process for tetraethyl orthosilicate (TEOS, n⩾2), (b) Digital images of the *in situ* generated silica/PAC co-gel.

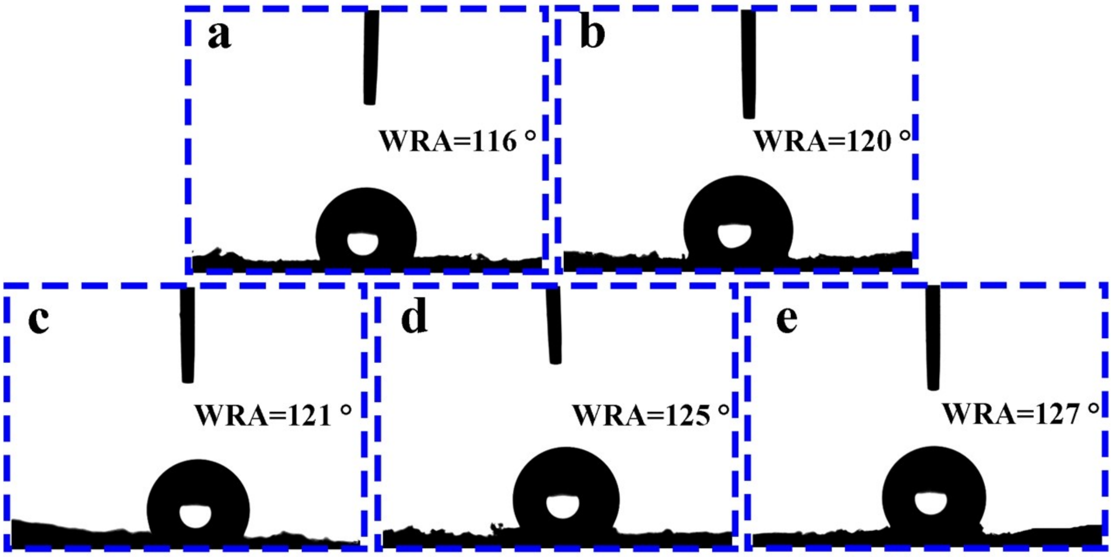

Figure S2. Water contact angle (WRA) of PI and SiO_2/PI-n aerogels. (a) PI aerogel. (b) SiO_2/PI-1 aerogel. (c) SiO_2/PI-2 aerogel. (d) SiO_2/PI-3 aerogel. (e) SiO_2/PI-4 aerogel.

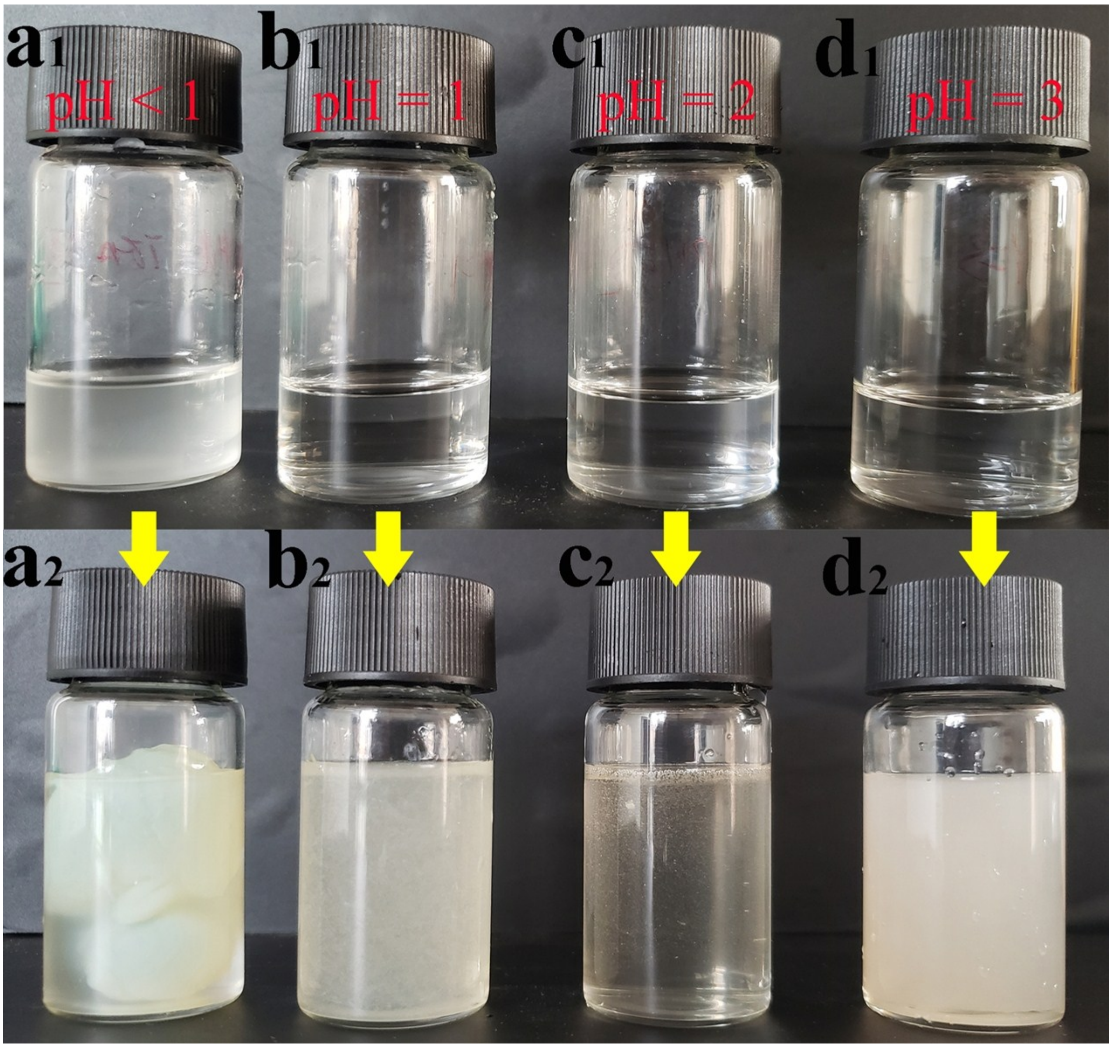

Figure S3. Digital images hydrolysate of TEOS under different pH value conditions and Digital images of the mixture of PAC and hydrolysate of TEOS correspondently. (a1and a2) Hydrolysis pH value of TEOS is lower than 1. (b1 and b2) Hydrolysis pH value of TEOS is 1. (c1 and c2) Hydrolysis pH value of TEOS is 2. (d1 and d2) Hydrolysis pH value of TEOS is 3.

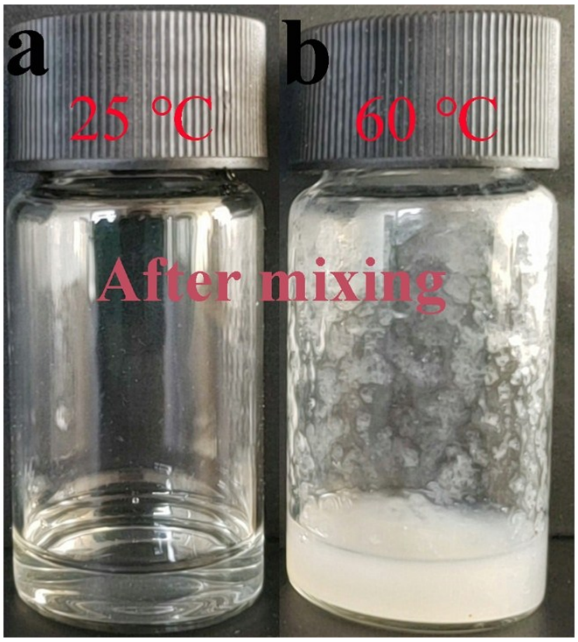

Figure S4. Digital images of the mixture of water-soluble PAC and hydrolysate of TEOS under different temperature conditions. (a) Hydrolysis temperature of TEOS is 25 ℃. (b) Hydrolysis temperature of TEOS is 60 ℃.

Figure S5. Morphology images of PI aerogel. The PI aerogel showed a disordered honeycombs-like porous structure and the wall of the pores exhibited smooth.

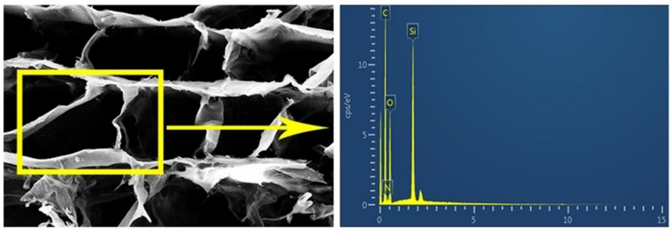

Figure S6. Morphology image of SiO_2/PI-3 aerogel for EDS mapping.

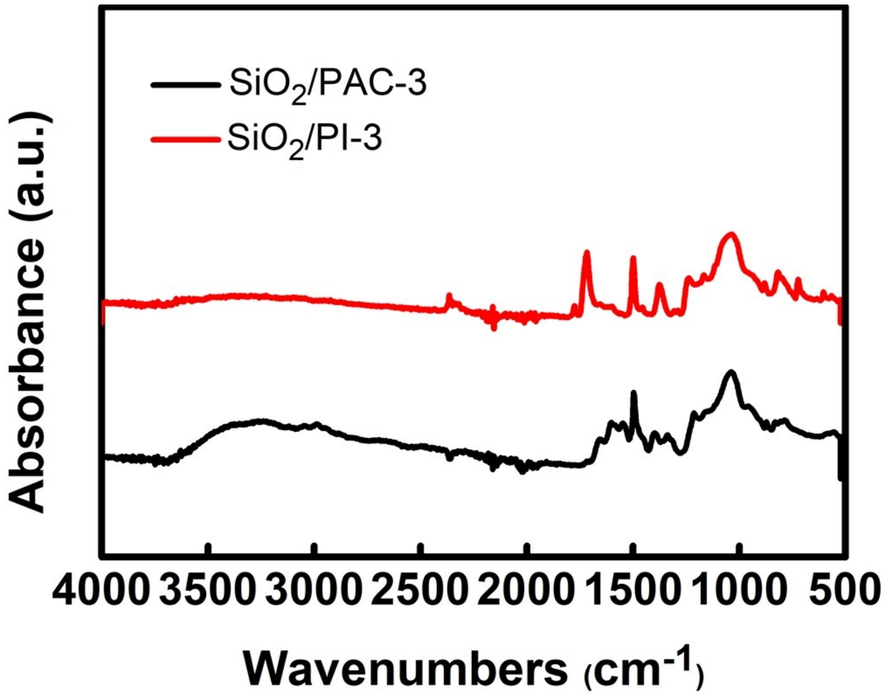

Figure S7. FTIR spectra of the SiO_2/PAC-3 and SiO_2/PI-3 aerogels.

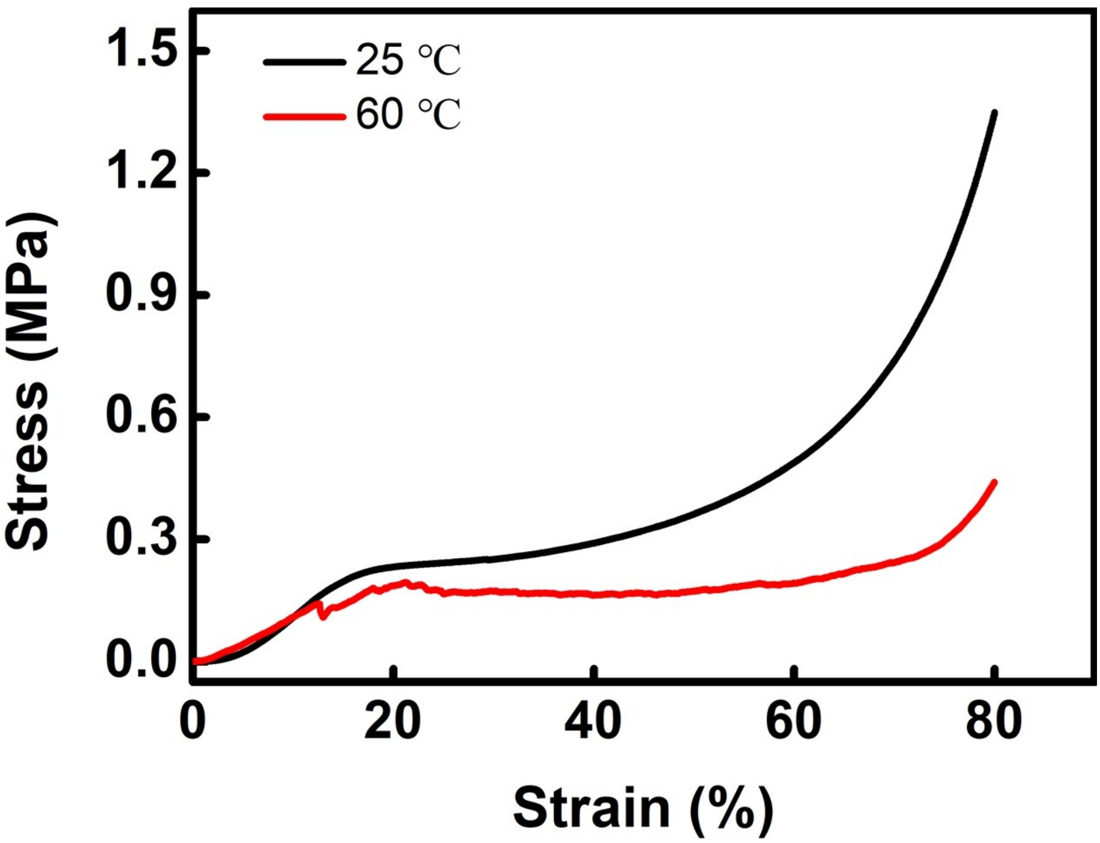

Figure S8. Compressive stress-strain (δ–ε) curves of SiO_2/PI-3 and SiO_2/PI-3-60 aerogels.

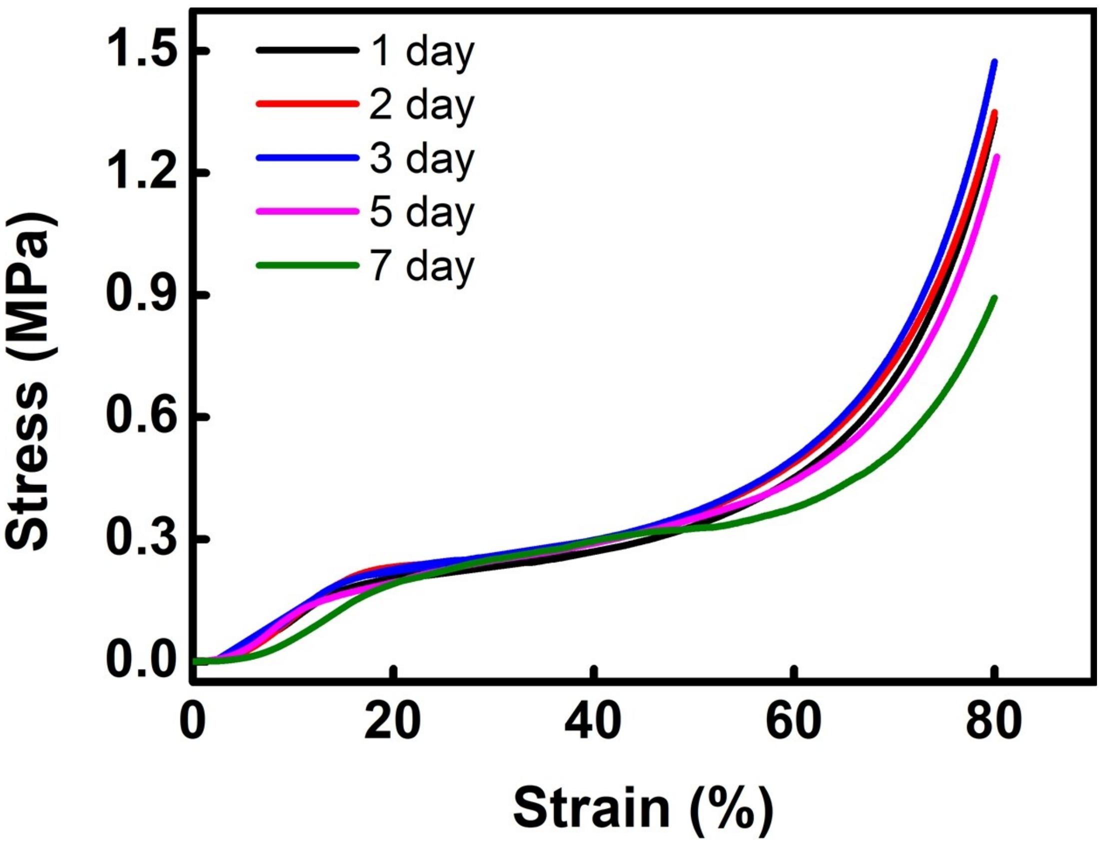

Figure S9. Compressive stress-strain (δ–ε) curves of SiO_2/PI-3, SiO_2/PI-3-1D, SiO_2/PI-3-3D, SiO_2/PI-3-5D, and SiO_2/PI-3-7D aerogels.

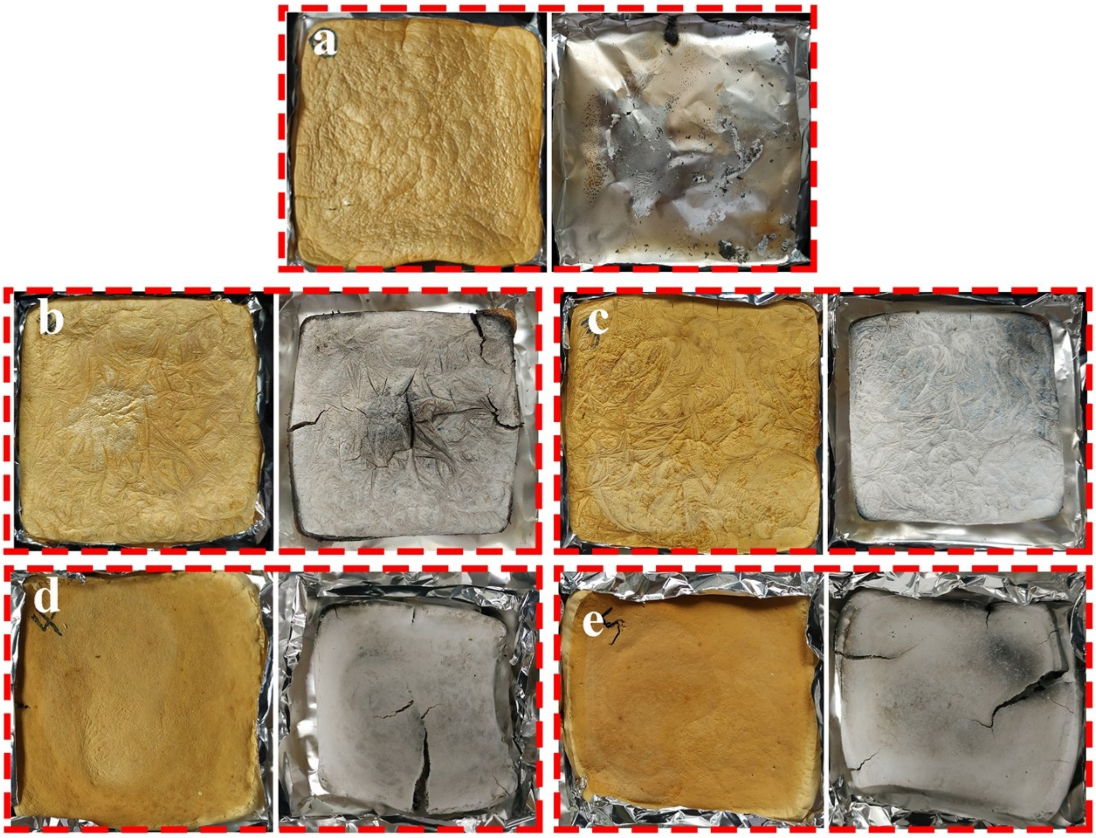

Figure S10. Digital images of pre-test and post-test of samples for flame. (a) PI aerogel. (b) SiO_2/PI-1 aerogel. (c) SiO_2/PI-2 aerogel. (d) SiO_2/PI-3 aerogel. (e) SiO_2/PI-4 aerogel.

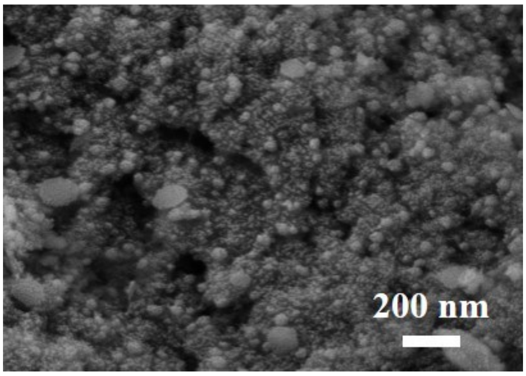

Figure S11. The morphology of the SiO_2/PI aerogel after burned.

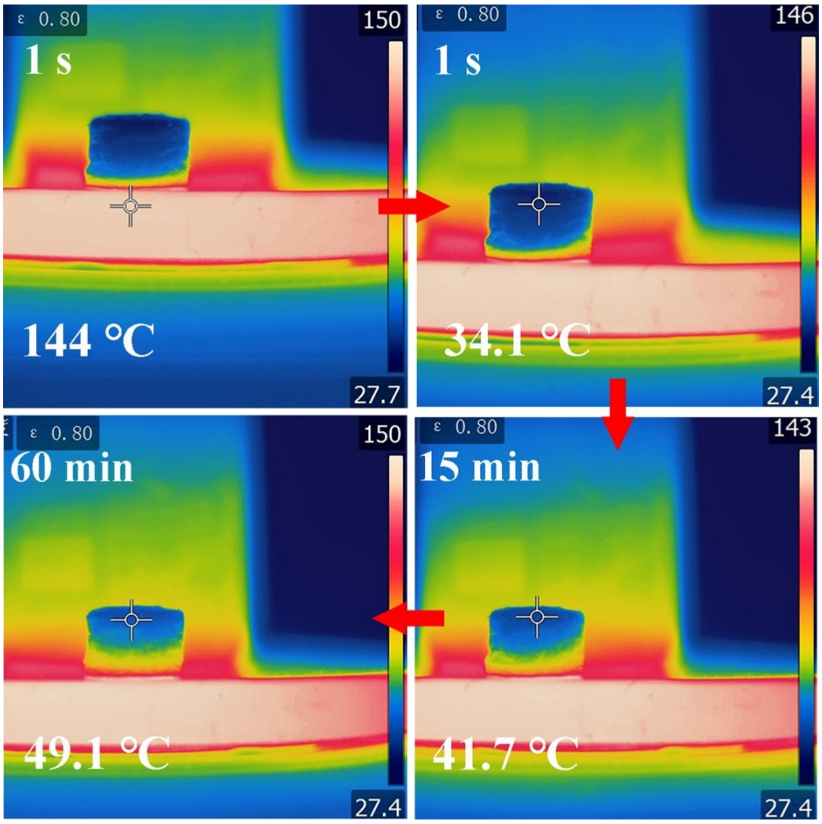

Figure S12. Infrared images of PI aerogel on a 144 °C heating stage.

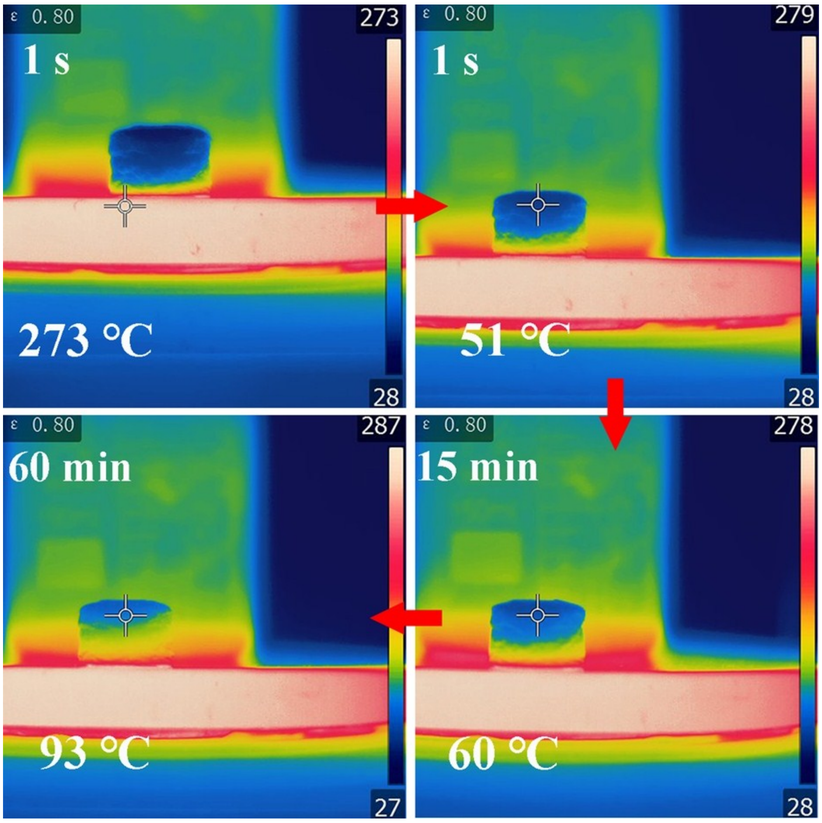

Figure S13. Infrared images of PI aerogel on a 273 °C heating stage.

Table S1. The detailed variable information for preparing silica/polyimide composite aerogels and the sample names.

Sample	TEOS (g)	pH value (water)	Hydrolysis temperature (℃)	Hydrolysis time (day)
SiO_2/PI-1	0.348	2	25	2
SiO_2/PI-2	0.696	2	25	2
SiO_2/PI-3	1.044	2	25	2
SiO_2/PI-4	1.392	2	25	2
—	1.044	< 1	25	2
—	1.044	1	25	2
—	1.044	2	25	2
—	1.044	3	25	2
SiO_2/PI-3-60	1.044	2	60	2
SiO_2/PI-3-1D	1.044	2	25	1
SiO_2/PI-3-3D	1.044	2	25	3
SiO_2/PI-3-5D	1.044	2	25	5
SiO_2/PI-3-7D	1.044	2	25	7

Table S2. Comparison of flame retardant of various organic and inorganic composite flame-resistant materials.

Sample	LOI	Heat flux ($kW\ m^{-2}$)	PHRR ($kW\ m^{-2}$)	TTPHRR (s)	FIGRA (W s)	THR ($MJ\ m^2$)	TSR ($m^2\ m^{-2}$)	Ref.
M5Pe5	35	50	80.1	65	1.2	19.7	~	1
PC/TiO_2@DPP50	29.7	50	412	65	6.3	20.5	~	2
RPUF-15	~	35	265.9	35	7.6	12.2		3
PU/Aerogel -0.7	60	50	220	36	6.3	19	964	4
PSi-70	~	35	19	~	~	0.55	~	5
FPU/Alag-20	~	50	71	14	5.1	3.8	38	6
PMMA/GAPPA	25	50	76	~	~	6.9	~	7
PI/G5/M10	55	50	52.5	52.5	1	10.7	18.4	8
A2.5C2.5-6	~	50	18.6	20	0.9	2.7	54.7	9
P5M3B	27.6	50	146	15	9.7	11.3	~	10
PI	34	50	84	40	2.1	8.6	84	**This work**
SiO_2/PI-1	43	50	52.9	90	0.6	6.2	59	
SiO_2/PI-2	44	50	42.2	105	0.4	5.2	44	
SiO_2/PI-3	47	50	36.6	115	0.3	4.1	29	
SiO_2/PI-4	48	50	30.7	130	0.2	3.2	20	

References

1 H. B. Chen, X. L. Li, M. J. Chen, Y. R. He, H. B. Zhao, *Carbohydr. Polym.*, 2019, **206**, 609-615.

2 Y. X. Wei, C. Deng, H. Chen, L. Wan, W. C. Wei, Y. Z. Wang, *ACS Appl. Mater. Interfaces*, 2018, **10**, 28036-28050.

3 S. X. Wang, H. B. Zhao, W. H. Rao, S. C. Huang, T. Wang, W. Liao, Y. Z. Wang, *Polymer*, 2018, **153**, 616-625.

4 H. B. Chen, P. Shen, M. J. Chen, H. B. Zhao, D. A. Schiraldi, *ACS Appl. Mater. Interfaces*, 2016, **8**, 32557-32564.

5 Z. L. Yu, N. Yang, V. Apostolopoulou-Kalkavoura, B. Qin, Z. Y. Ma, W. Y. Xing, C. Qiao, L. Bergström, M. Antonietti, S. H. Yu, *Angew. Chem., Int. Ed.*, 2018, **57**, 4538-4542.

6 H. Y. Xie, W. Yang, A. C. Y. Yuen, C. Xie, J. S. Xie, H. D. Lu, G. H. Yeoh, *Chem. Eng. J.*, 2017, **311**, 310-317.

7 L. Wang, S. H. Wu, X. Y. Dong, R. Wang, L. Q. Zhang, J. L. Wang, J. Zhong, L. X. Wu, X. Wang, *J. Mater. Chem. A*, 2018, **6**, 4449-4457.

8 L. Z. Zuo, W. Fan, Y. F. Zhang, L. Zhang, W. Gao, Y. P. Huang, T. X. Liu, *Compos. Sci. Technol.*, 2016, 139, 57-63.

9 X. L. Li, M. J. Chen, H. B. Chen, *Compos. Part B: Eng.*, 2019, 164, 18-25.

10 K. Shang, D. D. Ye, A. H. Kang, Y. T. Wang, W. Liao, S. Xu, Y. Z. Wang, *Polymer*, 2017, **131**, 111-119.